Innovative Systems Design and Engineering
ISSN 2222-1727 (Paper) ISSN 2222-2871 (Online)
Vol.4, No.13, 2013

Finite Element Analysis for Stress-Strain Parameter of Projectile Impeded Glass Fibre Reinforced Polyester (Gfrp) Composites

Onyechi, Pius C[1]., Edelugo, Sylvester O[2]., Ihueze, Chukwutoo C[1]., and Obuka, Nnaemeka, S.P[3]
1: Department of Industrial and Production Engineering, Nnamdi Azikiwe University, Awka, Nigeria.
2: Department of Mechanical Engineering, University of Nigeria, Nsukka, Nigeria.
3: Department of Mechanical and Production Engineering, Enugu State University of Science and Technology, Enugu, Nigeria.
Corresponding Author's email: silvermeks7777@yahoo.com. Tel: +234(0)8034002623

Abstract
For the treatment of progressive damage, spatial discretization is required so that numerical techniques such as the finite element method or finite difference method would be advantageous. Finite element and finite difference techniques have also been applied to impact problems because they are more versatile at modeling boundary conditions and local phenomena such as stresses and strain under a point load. This paper investigates the stress-strain magnitude on body amour composites of glass fibre reinforced polyester (GFRP), when hit with ogival and conical nosed projectiles through the application of finite element analysis using ANSYS software version 10.1. The finite element result of the plain stress analysis shows that the composite is stronger in the longitudinal direction. This is supported by the fact that the maximum stress of 328.125MPa was recorded in the X direction while the maximum stress of 57.726MPa was recorded in the Y direction. The analysis also indicates that the maximum influence of the stress was experienced around the incident hole and the minimum at the exterior boarders of the samples.
Keywords: Finite Element, Plain Stress Analysis, Projectiles, ANSYS Software, Body Amour, Fibre Reinforcement.

1. Introduction

The design of composite armour is a very complex task as compared to conventional single-layer metallic armour, due to the exhibition of coupling among membrane, torsion and bending strains, weak transverse shear strength and discontinuity of the mechanical properties along the thickness of the composite laminates. This has drawn attention of several researchers to study the penetration phenomenon in composite amours. The impact resistance and subsequent load-bearing capacity of composite depend on many factors such as fibre and matrix properties, fibre-matrix lay-up, number of layers or ply, thickness, and impact velocity. Cantwell and Morton [1] and Prewo [2] stated that the impact, resulting in complete penetration of laminate due to the high velocity is called ballistic impact and is of major concern to the armour designers. Further, the damage caused to the armour under high velocity impact is quite significant and has major effects on the dynamic properties of the laminates.

Laminated ballistic composite may be used in protective helmets or with ceramics and other materials like fibre reinforced polymers (FRP) for protective body amour [3]. The understanding of the behavior of laminated composite structures subjected to impact is an important as well as a complex problem. This is primarily due to dependency of a number of aspects such as material behavior, failure mechanisms, load transfer and with numerous uncertainties. As a result of this, the prediction of the impact behavior leads to an open problem, where investigations have been carried out in different ways ranging from simple empirical models to extremely sophisticated complex numerical techniques [4].

Impact, damage, penetration and perforation modeling of thick-section composites are of great importance to many industrial, automobile, aerospace and defense applications. A large number of material properties and model parameters are required in damage and impact modeling of composites using finite element analysis (FEA). A systematic model-experiment methodology is required to validate the finite element model (FEM) from static to impact

loading conditions [5]. A validated FEM should predict the evolution of impact damage, the rebound velocity of the projectile, and the impact-contact or resistance force for non-penetrating projectiles. For penetrating projectiles, the prediction of projectile residual velocity and displacement, evolution of damage, and penetration resistance force on projectile with significant accuracy is needed to predict the post-ballistic residual strength of the composite laminate and multi-hit performance. This paper investigates the stresses associated with the ballistic impact impeded on a glass fibre reinforced polyester matrix composite through the application of Finite Element Analysis (FEA).

2. Literature Review

There is significant interest within the engineering community to better understand and predict the damage sustained by composite structures under high energy ballistic impact. Ballistic survivability requirements are common in applications were structural integrity following high energy impact threats is critical to maintaining mission capability. A number of researchers [6–1O] have investigated the ballistic impact response of composite materials using a variety of numerical models and frameworks. Wang and Bartholomeusz [6] utilized the Dyna3D explicit finite element code to compare the measured and predicted ballistic impact damage of flat carbon/epoxy composite panels subjected to various small arms projectiles at velocities between 330 m/s and 1000 m/s over a range in obliquities. Silva et al [7] reported predictions of the ballistic impact of fragment simulating projectiles (FSPs) against thin Kevlar29/Vinylester panels at velocities of 320–360m/s. Their work utilized the AUTODYN finite difference code.

The relatively high complexity of impact problems is caused by the large number of intervening parameters like relative velocity of projectile and target, shape of colliding objects, relative stiffness and masses, time dependent surface of contact, geometry and boundary conditions and material characteristics [11; 12]. Difficulties increase when composite materials are involved, namely plates of FRP, due to orthotropy, larger variety of failure modes and uncertainties on constitutive laws. The finite-element method has recently been applied to two-dimensional impact problems involving severe distortion [13]. A comprehensive description of various finite-element methods is given in references works by [14 and 15]. The work presented herein is an extension of that presented in (Johnson, 1976) with the technique being extended for axisymmetric, two-dimensional, triangular elements to three-dimensional tetrahedron elements, [16]. Lee and Sun [17] used quasi-static finite element analysis to simulate the penetration process in the graphite/epoxy-laminate composites, where in the penetration criterion is based on statistic punch test. A variety of numerical techniques have been used to study and predict the behavior of composite laminates subjected to impact.

Both solid mechanics and fracture mechanics have been used to analyze impact phenomena. In the fracture mechanics approach, change is assumed to occur around an initiated crack due to stress concentrations at the crack tip. Therefore, decision must be taken where crack initiation has occurred and model local crack growth phenomena. In solid mechanics approach, fracture and local phenomena are averaged to model global structural behaviours. Damage is predicted when values of the stress or strain field satisfy a failure criterion. A solid mechanics approach will be taken for this analysis to model global processes rather than treating local phenomena such as fibre/matrix interation and inter-lamina boundary effects. There are many examples in the literature of analytical treatment of impact on composite.

For the treatment of progressive damage, spatial discretization is required so that numerical techniques such as the finite element method or finite difference method would be advantageous. Finite element and finite difference techniques have also been applied to impact problems because they are more versatile at modeling boundary conditions and local phenomena such as stresses and strain under a point load. Ghashghai-Abdi and Moyer [18] studied the difference between solution to impact problems with the finite element method and the

finite difference method in terms of performance and accuracy under scalar and vector processors. The finite element method was proven to be both faster and more accurate on scalar processors. Finite elements have also been proven to be superior in modeling complicated boundary and local loading conditions because of their functional form. They are also a useful tool for studying damage because of their ability to model local effects. There are many examples of finite element models applied to impact in the literature as shown by the comprehensive review in [19].

Finite element studies utilize both two and three dimensional techniques for modeling the response, damage, and sensitivity of composites. There are merits to both types of models. Two-dimensional analysis is less computationally an expense as the structures is assumed to respond in flexure. Three-dimensional analyses are used to study inter-lamina stresses and local phenomena. Bacharach and Hansen [20] used a three- dimensional model with a Hertziaz contact law to investigate damage to shells under impact. Damage was predicted by applying failure criteria to the calculated stress field. Ross et al. [21] used a three-dimensional approach with a ramp load to look at inter-laminar stresses during impact. They found that inter-laminar stresses were large at the onset of impact and were responsible for damage initiation. Chang et al. [22] used a two-dimensional plane-strain model to study stress and modes of failure of a composite beam under a line-load impact. They proposed a mechanism for damage where high inter-laminar stresses at the onset of impact caused matrix cracking which initiated de-lamination growth. Damage initiation was predicted by applying a matrix crack failure criterion to the stress field. Another notable result was that transverse normal stresses were small during impact, which implies that a flexural element would be appropriate for modelling impact.

Sun [23], Sun and Chen [24], Sun and Huang [25] derived a contact law for composites based on the Hertzian contact law and a flexural finite element model to study the response of composite plates and beams under impact. In particular, he examined the effects of pre-stress, impactor mass, velocity, and energy dissipation on impact behaviour. Humphreys [26] performed a finite element analysis of impact with a model failure criterion to predict damage progression in composites. In his model, he assumed that the impact was perfectly plastic and that there was no bending-extensional coupling in the model. Humphreys found that matrix cracking initiated due to high transverse shear stresses early in the impact event. Humphreys and Goering [27] then developed a model based on Mindlin plate theory and a Hertzian contact law to model the response of a plate under impact. They found that damage occurred at the early stage of the impact from inter-laminar failures due to very high moment gradients under the impactor. In general, impact analyses have been restricted to models in which damage is calculated peripherally to the stress calculations. To study the influence of various parameters affecting the penetration process in high velocity impact, the model should be able to describe the physical events, such as indentation, fibre breakage, de-lamination, bulging occurring during penetration.

3. Methodology And Applicable Materials

3.1 Experimental Procedure

Mixed methods of experimental and numerical methods were used. The class of glass fibres used in this work is the matted woven roving E-glass procured from NYCIL Chemical Industries Nkpor, Idemili North L.G.A., Anambra State, Nigeria. E-glass class, which is a low alkali Borosilicate was initially, developed for electrical application, hence the designation E. The diameter of each E-glass fibre is about 0.01 mm with an average length of 50mm. It has a density of 2550kg/m^3; Young's Modulus of 72 GN/m^3; and a strength of roughly 3.4 GN/m^2. The Polyester Resin used for this work was also procured from NYCIL. It services as the polymer matrix (greatest in percentage of the reagents) for the sample preparation. The speed at which the resin sets can be controlled by the quantity of catalyst and accelerator used.Methyl Ethyl Ketone Peroxide (MEKP), served as catalyst to the reaction process. Cobalt II Ethyl Hexanoate acted as an accelerator for the release of the free of radical that enhances curing by the catalyst. Paraffin Wax was applied on the surface of mould to enhance the ease removal of the prepared sample from the mould untampered. This is also called a releasing agent.

The hand lay-up method was used in formation of the composite materials. Here the polyester resin was applied on the mould evenly with the help of a hand brush to a thickness of about 1mm, then the woven roving fibres were lay-up in the mould and properly wetted out in a process known as fibre impregnation. More fibre plies were lay-up in the mould and compressed according to the required laminate thickness. For the thickness of 28

mm, 24 mm, 20 mm, 16 mm, 12mm and 8mm, the number of plies were 22, 18, 15, 12, 9, and 6 respectively. The fibre content by volume fraction varies from 0.48 to 0.50.

3.1.1. Penetration of Semi-Infinite GFRP Laminates

The types of projectiles (life bullets) that were used are the rigid projectile with ogival and conical nosed.

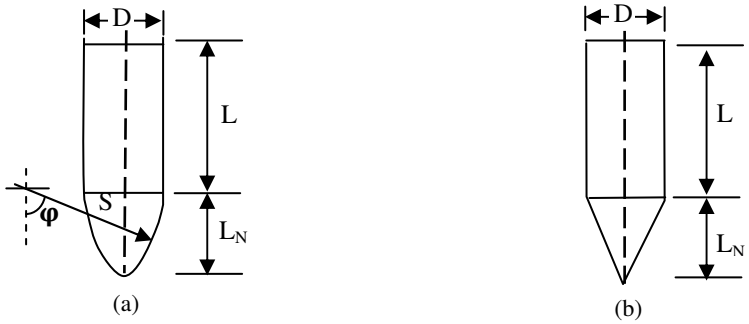

Fig. 1: Projectile geometries (a) Ogival nose and (b) Conical nose

The projectiles are assumed to have density ρ_p and mass M with diameter D (or radius r), L and L_N are the lengths of the shank and nose of ogival and conical projectile as shown in Fig 1. Fig 1(a) shows the ogive profile as the arc of the circle(s) that is tangent to the shank. It is also common to define the ogive in terms of caliber – radius – head.

$$CRH = \frac{S}{2r} = \psi \qquad (1)$$

Six composite laminate armour sample plates of size 300mm by 400mm and thicknesses of 8mm, 12mm, 16mm, 20mm, 24mm and 28mm were targeted using two types of life bullets (Ogival and Conical nosed) of equal diameter and mass. The rifle used was the Beretta Cal 9 x 19 parabellum models 951 of muzzle velocity of 355m/s and the angle of attack was 0^0(normal). Figs. 2 to 7 show the ballistic impact, perforation and penetration on the six GFRP composite laminate samples.

Fig. 2: Sample E, showing complete absorption of impact.

Fig 3: Sample D, showing minimal shattering by impact.

Fig. 4: Sample C, showing some shattering and penetration, but no perforation.

Fig. 5: Sample B, showing sign of penetration but no perforation.

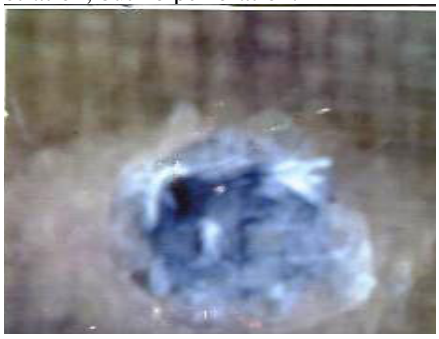

Fig. 6: Sample A, showing heavy shattering but no perforation

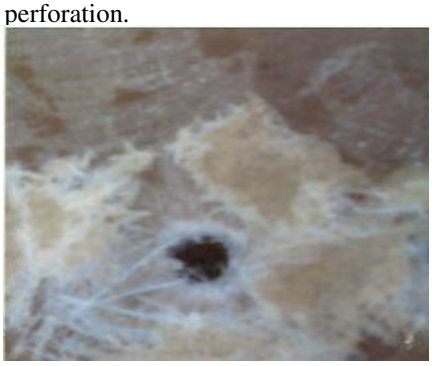

Fig. 7: Sample F, showing failure with complete perforation.

It was observed that five samples resisted or arrested the assault of the projectiles while the sixth sample failed (the bullets went through). The distance between the target and the gun was measured to be 50meters.
The classification of the bullet used is shown in the Table 1.

Table 1: Classification of Bullets used

Parameter	Ogival	Conical
Projectile Caliber	22 (5.6 mm)	45^{o} conical tipped
Cartridge size Type	27grain	27grain
Nominal Type	1.7gram	1.7gram
Bullet diameter	5.7mm	5.7mm
Velocity	355m/s	355m/s
Effective range	200meters	200meters
Mass Density of Bullet	11,400kg/m^{3}	11,400kg/m^{3}

Source: Wikipedia, the free encyclopedia.

3.2 MATERIAL STRENGTH

3.2.1 Stress Analysis with Finite Element

Before contemplating on using finite elements for stress analysis one has to understand very well classical stress analysis method and the available material behavior models as may be available in most solid mechanics texts. In the previous section, the derivation of shape equation or interpolation functions of some typical elements. The shape function matrix was also established and can be reduced to;

$$U^{e} = N^{e}d^{e} \qquad (2)$$

In this section the usefulness of shape function and shape matrixes should be utilized in the analysis of plane stress, plane strain and axisymmetric stress analysis of continuums and structural elements. Plane stress concerns

a body which is thin in the ~~Z~~-direction and plane strain for body that is along the ~~Z~~-direction while axisymmetric is for bodies' revolution as depicted in Figs. 8(a), (b), and (c) respectively.

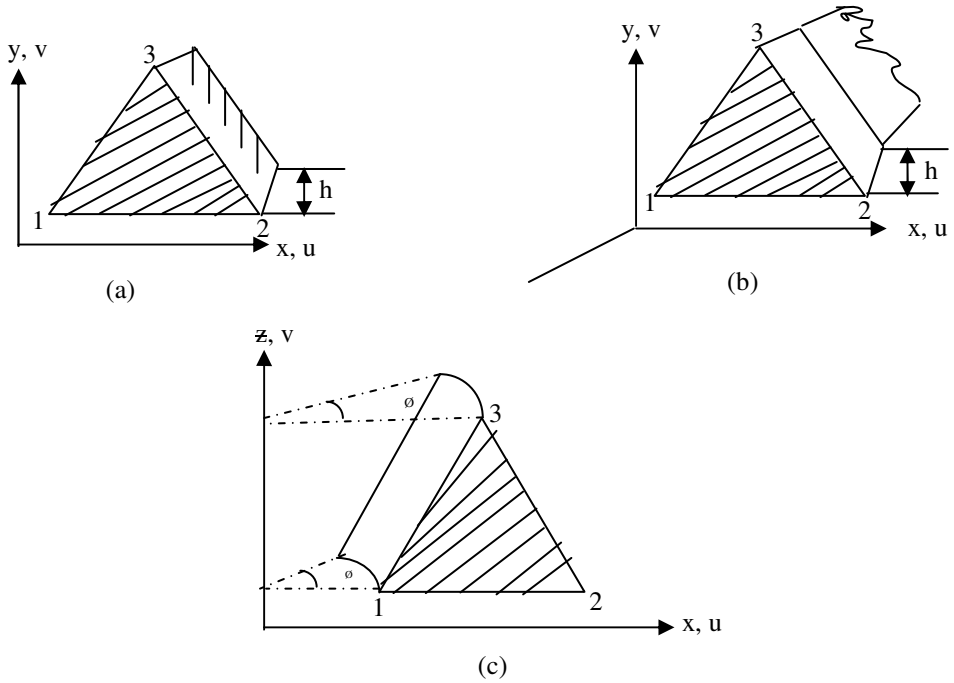

Fig 8: Shape function of Plain Stress, Plain Strain and Axisymmetric Stress.

Generally, plane stress analysis is for components or structures which are then in the ~~Z~~-direction, while plane stain analysis is for components which is long or infinite the ~~Z~~–direction and axisymmetric analysis for bodies which have axis of symmetry or for bodies of revolution. Axisymmetric elements which could be linear or quadratic as

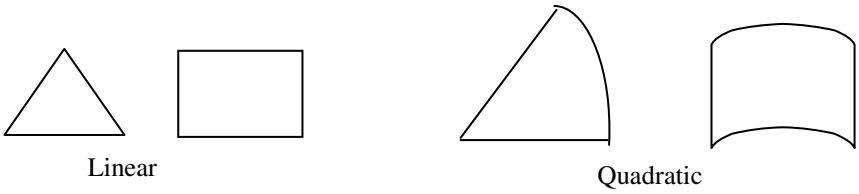

Fig 9: Axisymmetric Elements

Common mistakes which are often made novice FE user when applying axisymmetric remarks is to note place the model in the correct location in the global coordinate system. The correct positions as suggested [28] is as shown in Fig 10,

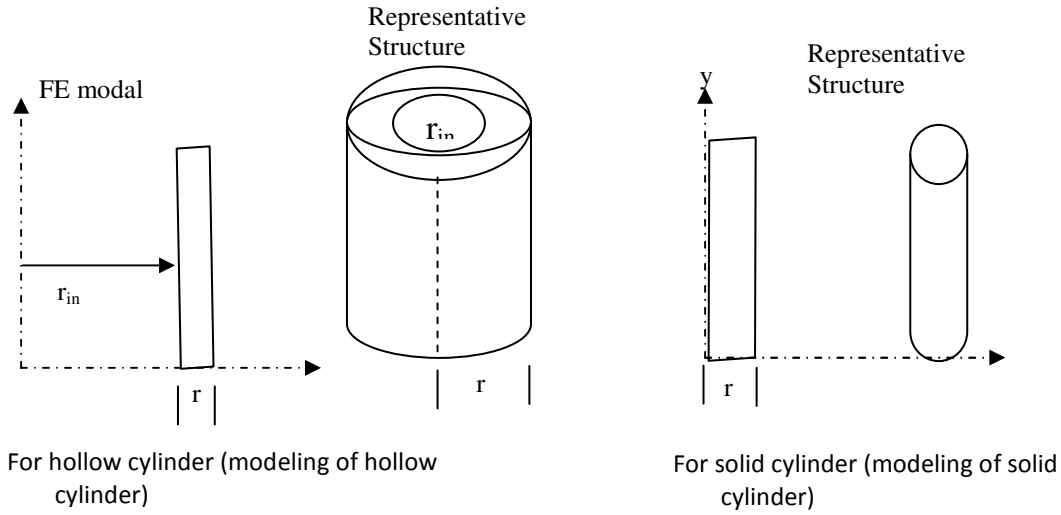

Fig 10: Hollow and Solid Cylinder Model

It is this FE model that is then discretized using a selected element type (linear or quadratics). In the plane stress, plane strain and axisymmetric stress analysis, a solid area surface is subdivided and not volume so that the problem is described as two dimensional.

3.2.2 Plane Stress analysis

By considering an isolated triangular Element whose nodes are ordered counter clockwise the shape functions and shape matrixes are established after the evaluation of shape constants on the assumption of two dimensional problem linear in x and y

Strain displacement relationship: Plane Stress analysis starts by considering strains in x and y directions and working on the shape or interpolation function of equation (2) by taking partial derivatives:

$$\left.\begin{aligned} \varepsilon_x &= \frac{\partial u}{\partial x} = \frac{\partial n_1}{\partial x}U_1 + \frac{\partial n_2}{\partial x}U_2 + \frac{\partial n_3}{\partial x}U_3 \\ \varepsilon_y &= \frac{\partial v}{\partial y} = \frac{\partial n_1}{\partial y}V_1 + \frac{\partial n_2}{\partial y}V_2 + \frac{\partial n_3}{\partial y}V_3 \\ \gamma_{xy} &= \frac{\partial u}{\partial y} + \frac{\partial v}{\partial x} = \frac{\partial n_1}{\partial y}U_1 + \frac{\partial n_2}{\partial y}U_2 + \frac{\partial n_3}{\partial y}U_3 + \frac{\partial n_1}{\partial x}V_1 + \frac{\partial n_2}{\partial x}V_2 + \frac{\partial n_3}{\partial x}V_3 \end{aligned}\right\} \quad (3)$$

When ε_x, ε_y and γ_{xy} = in plane stains expressed in terms of displacements. Equation (3) can be expressed in matrix form as;

$$\begin{bmatrix} \varepsilon_x \\ \varepsilon_y \\ \gamma_{xy} \end{bmatrix} = \begin{bmatrix} \partial n_1/\partial x & 0 & \partial n_2/\partial x & 0 & \partial n_3/\partial x & 0 \\ 0 & \partial n_1/\partial y & 0 & \partial n_2/\partial y & 0 & \partial n_3/\partial y \\ \partial n_1/\partial x & \partial n_1/\partial x & \partial n_2/\partial y & \partial n_2/\partial x & \partial n_3/\partial y & \partial n_3/\partial x \end{bmatrix} \begin{bmatrix} U_1 \\ V_1 \\ U_2 \\ V_2 \\ U_3 \\ V_3 \end{bmatrix} \quad (4)$$

But by taking partial derivatives of equation (3.23) expressed as $N_i(x,y) = \frac{1}{2A}(a_i + b_i x + c_i y)$, for i = 1, 2, 3 so that: For node i =1, 2, 3

$$\partial n_1/\partial x = \frac{1}{2A}(b_1), \quad \partial n_1/\partial y = \frac{1}{2A}(c_1)$$

$$\partial n_2/\partial x = \frac{1}{2A}(b_2), \quad \partial n_2/\partial y = \frac{1}{2A}(c_2)$$

$$\partial n_1/\partial x = \frac{1}{2A}(b_1), \partial n_1/\partial y = \frac{1}{2A}(c_1)$$

$$\begin{bmatrix} \varepsilon_x \\ \varepsilon_y \\ \gamma_{xy} \end{bmatrix} = \frac{1}{2A}\begin{bmatrix} b_1 & 0 & b_2 & 0 & b_3 & 0 \\ 0 & c_1 & 0 & c_2 & 0 & c_3 \\ c_1 & b_1 & c_2 & b_2 & c_3 & b_3 \end{bmatrix}\begin{bmatrix} U_1 \\ V_1 \\ U_2 \\ V_2 \\ U_3 \\ V_3 \end{bmatrix} \qquad (5)$$

Equation can be written as;

$$\varepsilon = B^e d^e \qquad (6)$$

e is called the strain displacement matrix. Since all the components of B^e are constants, the strains are constant. The element is therefore referred as the constant strain triangle (CST).

Stress-Strain Relationship: The conventional stress-strain relationship when a uni-axial and tri-axial stresses are applied to an isolated element are as shown in Fig 11.

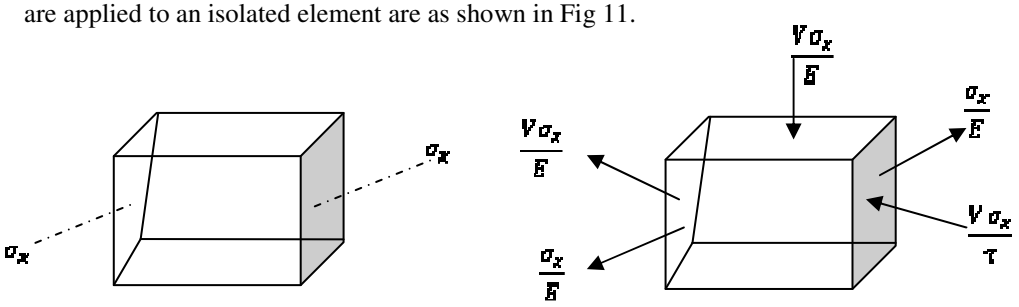

(a) Stress (b) Strain

Fig.11: Uni-axial Stress-Strain System

For a uni-axial stress-strain

$$\left.\begin{aligned} Ex &= \frac{\sigma_x}{E} \\ Ey &= -\frac{V\sigma_x}{E} \\ Ez &= -\frac{V\sigma_x}{E} \end{aligned}\right\} \qquad (7)$$

The negative sign indicates contraction for a tri-axial stress-system

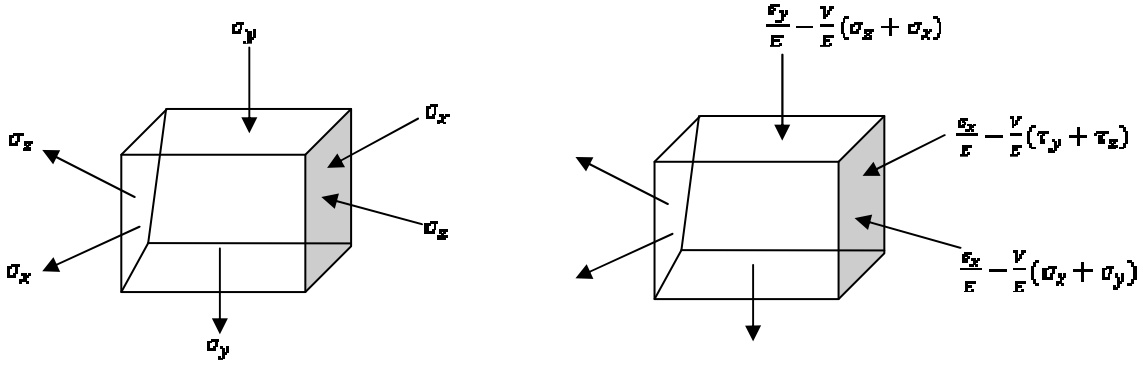

Fig 12: Tri-axial Stress –Strain System

So that the general stress-strain relationship can be expressed as;

$$\left.\begin{aligned} \varepsilon_x &= \frac{\sigma_x}{E} - \frac{V}{E}(\sigma_y + \sigma_z) \\ \varepsilon_y &= \frac{\sigma_y}{E} - \frac{V}{E}(\sigma_z + \sigma_x) \\ \varepsilon_z &= \frac{\sigma_z}{E} - \frac{V}{E}(\sigma_x + \sigma_y) \end{aligned}\right\} \quad (8)$$

When thermal strain is included, the expressions are reduces to;

$$\left.\begin{aligned} \varepsilon_x &= \frac{\sigma_x}{E} - \frac{V}{E}(\sigma_y + \sigma_z) + \alpha T \\ \varepsilon_y &= \frac{\sigma_y}{E} - \frac{V}{E}(\sigma_z + \sigma_x) + \alpha T \\ \varepsilon_z &= \frac{\sigma_z}{E} - \frac{V}{E}(\sigma_x + \sigma_y) + \alpha T \\ \gamma_{xy} &= \frac{2(I+V)}{E}\tau_{xy} \end{aligned}\right\} \quad (9)$$

The above stress-strain relationships are based on Hook's law of elasticity. The stress of equation (9) can be expressed as;

$$\left.\begin{aligned} \sigma_x &= \frac{E}{1-V^2}\left[(\varepsilon_x - \alpha T) + V(\varepsilon_y - \alpha T)\right] \\ \sigma_y &= \frac{E}{1-V^2}\left[(\varepsilon_y - \alpha T) + V(\varepsilon_x - \alpha T)\right] \\ \tau_{xy} &= \frac{E}{2(1+V)}\gamma_{xy} \end{aligned}\right\} \quad (10)$$

When σ_z, τ_{xz} and τ_{yz} are set equal to zero. The permit the analysis of plane stress which is the plane of x, y since ε is also assured to be minimal for plane stress analysis.

Equation (10) can be written in matrix form as

$$S = D[\varepsilon - \varepsilon_T] \quad (11)$$

Where,

$$S = \begin{bmatrix} \sigma_x \\ \sigma_y \\ \tau_{xy} \end{bmatrix}, \varepsilon = \begin{bmatrix} \varepsilon_x \\ \varepsilon_y \\ \gamma_{xy} \end{bmatrix}, \varepsilon_T = \begin{bmatrix} \alpha T \\ \alpha T \\ 0 \end{bmatrix} \quad (12)$$

And

$$D = \left(\frac{E}{(1-\nu^2)}\right)\begin{bmatrix} 1 & \nu & 0 \\ \nu & 1 & 0 \\ 0 & 0 & (1-\nu)/2 \end{bmatrix} \quad (13)$$

Where E = elastic modules and ν is the Poisson's ratio. Equation (13) gives the modules matrix (property matrix) which contains the basic properties of the element material.

Stiffness matrix: The stiffness matrix of an element constant with element nodes is classically expressed as;

$$K^e = \int_v B^{eT} D B^e dV \quad (14)$$

Since B^e and D are constant matrixes and B^{eT} is the transpose of B^e and $dV = AT$ where A = element area and T is the element thickness, the integrand of (14) can be taken as;

$$K^e = (AT)\, B^{eT} D B^e \quad (15)$$

The equivalent thermal forces applied to element nodes are evaluated with,

$$f_T^e = \int_v (B^{eT} D \varepsilon_T) dV \quad (16)$$

While the equivalent body forces are evaluated with,

$$f_T^e = \int_v (N^{eT} g) dV \quad (17)$$

If the temperature change is uniform over the element, all the terms of expression (16) are constant and the thermal load vector can be expressed as;

$$f_T^e = (AT) B^{eT} D \varepsilon_T \quad (18)$$

In physical terms, f_f^e is a b X l vector whose components represent equivalent forces which must be applied to the modes of the element in the directions of $U_1 V_1$, $U_2 V_2$, and $U_3 V_3$. The evaluation of body force vector f_g^e is not straight forward because the integrand is no longer constant since the components of the shape matrix N^e are linear functions of x and y. Provided that the thickness of the element is constant, expression (16) can be expressed as;

$$f_g^e = T \int_A (N^{eT} g) dx dy \qquad (19)$$

By inserting the components of N^e and g then

$$f_g^e = T \int_A \begin{bmatrix} n_1 & 0 \\ 0 & n_1 \\ n_2 & 0 \\ 0 & n_2 \\ n_3 & 0 \\ 0 & n_3 \end{bmatrix} \begin{bmatrix} g_x \\ g_y \end{bmatrix} dx\, dy = T \int_A \begin{bmatrix} n_1 g_x \\ n_1 g_y \\ n_2 g_x \\ n_2 g_y \\ n_3 g_x \\ n_3 g_y \end{bmatrix} dx \qquad (20)$$

The individual components of f_g^e have the dimensions of force and correspond must be applied at the nodes of the element. You can see that the first, third and fifth components act in the directions of U_1, U_2 and U_3 while, the second, fourth and sixth act in the directions of V_1, V_2 and V_3. This understanding is very important. The equivalent nodal forces in the x and u directions at each node can be written as;

(a) $T \int_A n_i(x,y) g_x d_x d_y, (i = 1, 2, 3)$, in the x-direct

and

(b) $T \int_A n_i(x,y) g_y d_x d_y, (i = 1, 2, 3)$, in the y-direct

If the body force is constant over the element, integrals (a) and (b) reduce to $(1/3)\ G_x$ and $(1/3)\ G_y$ respectively while G_x and G_y are resultant forces in the x and y directions.

3.2.3 Plane Strain Analysis

This is suited for component long or infinite in the ~~z~~-direction. But in the plane strain the assumption of zero normal stress, σ_z is replaced by an assumption that e_z is zero.

$e_z = 0$ So that for plane strain situation

$$\left.\begin{aligned} e_x &= \frac{1}{E}[\sigma_x - V\sigma_y - V\sigma_z] + \propto T \\ e_y &= \tfrac{1}{E}[\sigma_y - V\sigma_x - V\sigma_z] + \propto T \\ 0 &= \frac{1}{E}[\sigma_z - V\sigma_x - V\sigma_y] + \propto T \end{aligned}\right\} \qquad (21)$$

and

$$\gamma_{xy} = \tau_{xy}(1 + V)\, 2/E$$

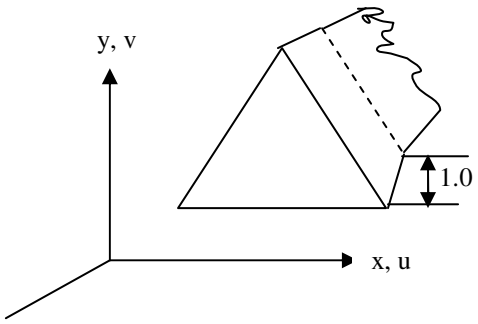

Fig 13: Plain Strain Element

The axial stress σ_z may be eliminated for equation (21) and the remaining equations inverted to obtain,

$$\sigma_x = \frac{E(1-V)}{(1+V)(1-2V)}\left[\varepsilon_x + \left(\frac{V}{1-V}\right)\varepsilon_y - \left(\frac{1+V}{1-V}\right)\propto T\right]$$
$$\sigma_y = \frac{E(1-V)}{(1+V)(1-2V)}\left[\varepsilon_y + \left(\frac{V}{1-V}\right)\varepsilon_x - \left(\frac{1+V}{1-V}\right)\propto T\right] \quad (22)$$
$$\tau_{xy} = \frac{E}{2(1+V)}\gamma_{xy}$$

By putting (22) in standard matrix form as usual,

$S = D[\varepsilon - \varepsilon_T]$

Where,

$$S = \begin{bmatrix}\sigma_x\\ \sigma_y\\ \tau_{xy}\end{bmatrix}, \varepsilon = \begin{bmatrix}\varepsilon_x\\ \varepsilon_y\\ \gamma_{xy}\end{bmatrix} \quad (23)$$

Where the stress-strain matrix (D) also called modules or property matrix is given as

$$D = \frac{E(1-V)}{(1+V)(1-2V)}\begin{bmatrix}1 & V/(1-V) & 0\\ V/(1-V) & 1 & 0\\ 0 & 0 & \frac{1}{2}(1-2V)/(1-V)\end{bmatrix} \quad (24)$$

Note that the thickness of the element in the z direction is not always clearly defined in the case of pane strain, since the theory apply in principle to bodies which are in determinately long. A definite value is required in all element integrals and is conveniently taken to be unity in the absence of other information. The plane stress and plane stress analysis of this text follow this approach [29 and 30].

3.2.4 Axisymmetric Stress Analysis.

The axisymmetric element represents a sector of a triangular annulus that the modifications which must be made to linear triangle for axisymmetric use are somewhat more extensive.

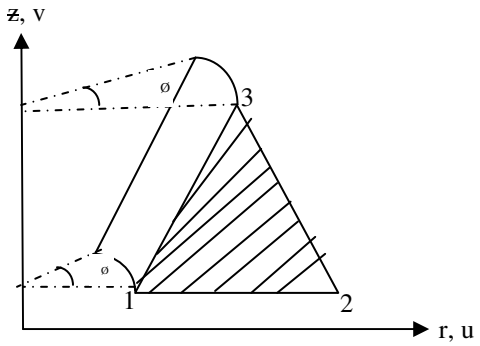

Fig 14: Axisymmetric Element

The x and y co-ordinates of the original plane stress representation are then replaced by radial and axial polar coordinates, r and z since the nodal values of the functions are still defined by U_1, V_1, U_2, V_2, U_3 and V_3. The shape function for U and V are identical to those of plane stress except that the Cartesian coordinates x and y are replaced by r and z so that we can write

$$\begin{bmatrix}U\\ V\end{bmatrix} = \begin{bmatrix}n_1(r,z) & 0 & n_2(r,z) & 0 & n_3(r,z) & 0\\ 0 & n_1(r,z) & 0 & n_2(r,z) & 0 & n_3(r,z)\end{bmatrix}\begin{bmatrix}U_1\\ V_1\\ U_2\\ V_2\\ U_3\\ V_3\end{bmatrix} \quad (25)$$

Where

$$n_i(r,z) = 1/2A\,[a_i + b_i r + c_i z], \quad (i = 1,2,3) \tag{26}$$

Since x_i and y_i are replaced by strain by writing the shape equations as;

$$U = n_1(r,z)u_1 + n_2(r,z)u_2 + n_3(r,z)u_3$$

And

$$U = n_1(r,z)v_1 + n_2(r,z)v_2 + n_3(r,z)v_3$$

And taking partial derivatives, then

$$\left.\begin{aligned} \varepsilon_r &= \frac{\partial u}{\partial r} = \frac{\partial n_1}{\partial r}U_1 + \frac{\partial n_2}{\partial r} + \frac{\partial n_3}{\partial r}U_3 \\ \varepsilon_z &= \frac{\partial v}{\partial z} = \frac{\partial v}{\partial z}V_1 + \frac{\partial n_2}{\partial z}V_2 + \frac{\partial n_3}{\partial z}V_3 \\ \varepsilon_\theta &= \frac{u}{r} = \frac{n_1}{r}U_1 + \frac{n_2}{r}U_2 + \frac{n_3}{r}U_3 \\ \gamma_{r,z} &= \frac{\partial v}{\partial z} + \frac{\partial u}{\partial r} = \frac{\partial n_1}{\partial r}V_1 + \frac{\partial n_2}{\partial r}V_2 + \frac{\partial n_3}{\partial r}V_3 + \frac{\partial n_1}{\partial z}U_1 + \frac{\partial n_2}{\partial z}U_2 + \frac{\partial n_3}{\partial z}U_3 \end{aligned}\right\} \tag{27}$$

So equation (27) is expressed in matrix form, thus;

$$\varepsilon = \begin{bmatrix} \varepsilon_r \\ \varepsilon_z \\ \varepsilon_\theta \\ \gamma_{r,z} \end{bmatrix} = \begin{bmatrix} \partial n_1/\partial r & 0 & \partial n_2/\partial r & 0 & \partial n_3/\partial r & 0 \\ 0 & \partial n_1/\partial z & 0 & \partial n_2/\partial z & 0 & \partial n_3/\partial z \\ n_1/r & 0 & n_2/r & 0 & n_3/r & 0 \\ \partial n_1/\partial z & \partial n_1/\partial r & \partial n_2/\partial z & \partial n_2/r & \partial n_3/\partial z & \partial n_3/\partial_2 \end{bmatrix} \begin{bmatrix} U_1 \\ V_1 \\ U_2 \\ V_2 \\ U_3 \\ V_3 \end{bmatrix} \tag{28}$$

4 x 6 matrixes on the right of equation (28) defines B^e matrix for the element, replacing the analogous 3 x 6 matrix for the case of plane stress. Where the expressions for $n_1\,(r,z)$ are substituted into B^e, then

$$B^e = \frac{1}{2A}\begin{bmatrix} b_1 & 0 & b_2 & 0 & b_3 & 0 \\ 0 & c_1 & 0 & c_2 & 0 & c_3 \\ \dfrac{(a_1 + b_1 r + c_1 z)}{r} & 0 & \dfrac{(a_2 + b_2 r + c_2 z)}{r} & 0 & \dfrac{(a_3 + b_3 r + c_3 z)}{r} & 0 \\ c_1 & b_1 & c_2 & b_2 & c_3 & b_3 \end{bmatrix} \tag{29}$$

Stress-Strain relationship: By employing polar coordinates in the former Cartesian Stress-Strain relation of Hooks law and setting $\tau_{r\theta}$ and $\tau_{z\theta}$ to zero, Astley [29] had shown that;

$$S = D[\varepsilon - \varepsilon_T] \tag{30}$$

Where

$$S = \begin{bmatrix} \sigma_r \\ \sigma_z \\ \sigma_\theta \\ \tau_{xy} \end{bmatrix}, \varepsilon = \begin{bmatrix} \varepsilon_r \\ \varepsilon_z \\ \varepsilon_\theta \\ \gamma_{xz} \end{bmatrix}, \varepsilon_T = \begin{bmatrix} \alpha_T \\ \alpha_T \\ \alpha_T \\ 0 \end{bmatrix} \tag{31}$$

And

$$D = \frac{E(1-V)}{(1+V)(1-2V)}\begin{bmatrix} 1 & \dfrac{V}{(1-V)} & \dfrac{V}{(1-V)} & 0 \\ \dfrac{V}{(1-V)} & 1 & \dfrac{V}{(1-V)} & 0 \\ \dfrac{V}{(1-V)} & \dfrac{V}{(1-V)} & 1 & 0 \\ 0 & 0 & 0 & \dfrac{(1-2V)}{2(1-V)} \end{bmatrix} \tag{32}$$

The stiffness matrix can be evaluated with the integral

$$K^e = \int_v (B^{eT} D B^e)\,dV \tag{33}$$

And if the angle θ is taken to be one radian, the volume differential dV becomes $r\,dr\,dz$ and the stiffness matrix is,

$$K^e = \int_A B^{eT} D B^e r\,dr\,dz \tag{34}$$

Similarly the thermal load and body force vectors can be evaluated with the relations

$$f_T^e = \int_v (B^{eT} D B^e) dV \qquad (35)$$

$$f_B^e = \int_v (N^{eT} g) dV \qquad (36)$$

Respectively equation (35) and (36) are however modified in a similar manner to (34). The integration of these quantities is no longer trivial. Each integrand contains the factor r, and the matrix has a row of non constant terms. Analytic integration is difficult but we approximate integration by evaluating the integrand at the centroid of the element and simply multiply it by the area of integration.

4. The Finite Element Analysis Using ANSYS Software Version 10.1: Results and Discussion

As a result of the ballistic impact on the samples (of thicknesses; 8mm, 12mm, 16mm, 20mm, 24mm, and 28mm) the influence of the local as well as global stresses, strains and displacements were presented in Figs. 15 to 24. The material properties were imputed on the finite element model to obtain the values of stresses on the discretized nodes as shown in Figs. 15 to 24. The number of nodes considered is 7596 for 12mm thickness and 15192 for 24mm thickness. The minimum and maximum values of stresses, strains and displacements were also show in Figs. 15 to 24.

4.1 Plane Stress Analysis for 12mm Plate

The associated experimental data are, UTS = 145MPa; E = 20.64 GPa = 20.64E9 Pa, v = 0.38, L = 400mm; B = 300mm; Dia= 2.85mm.

The finite element results of plane stress analysis employing ANSYS are depicted in the following Figs. 15 to 19. Fig. 15 with maximum stress of 328.125MPa in the X direction shows that the composite is weaker in Y direction with maximum stress of 57.726MPa. Also Fig. 17 depicting von Mises stresses gives the yield stresses of various nodes describing the random yield strength of composites ranging from 96.19MPa to 304.084MPa. Fig. 18 and Fig. 23 are vector plots and displacement depiction for various nodes.

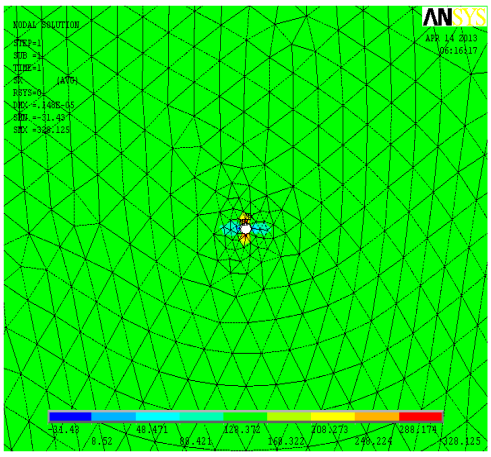

Fig. 15: Finite element model and depiction X component stresses

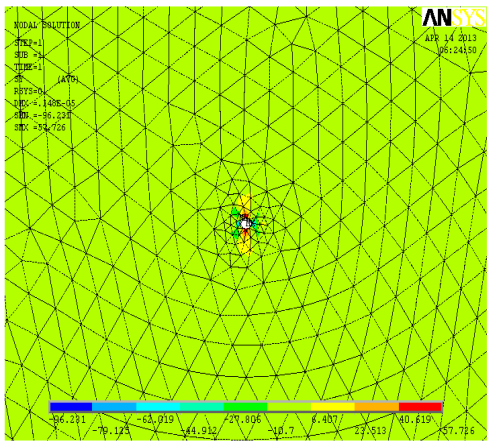

Fig. 16: Finite element model and depiction Y component stresses

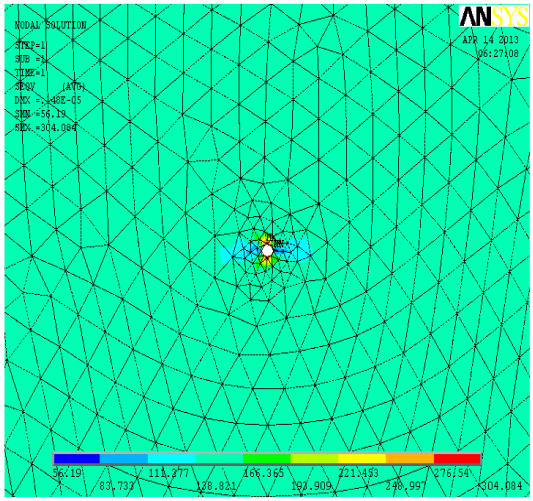

Fig. 17: Finite element model and depiction von Mises stresses

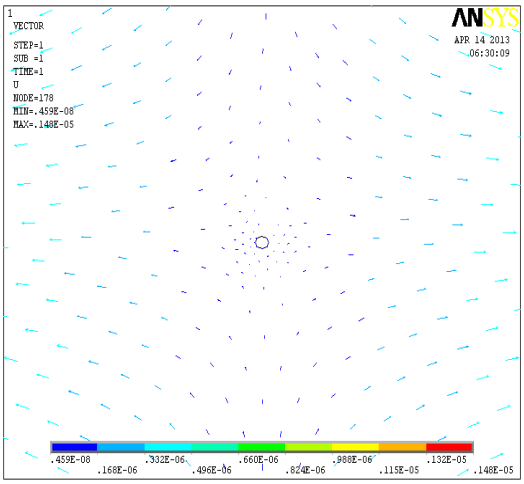

Fig. 18: Finite element model and depiction of vector/displacement plots

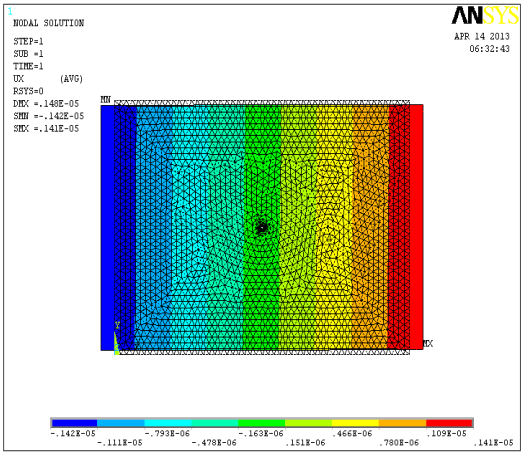

Fig. 19: Finite element model and depiction of nodal Strain plots

4.2 Plane Stress Analysis for 24mm Plate

The associated experimental data are, UTS = 145MPa; E = 20.64 GPa = 20.64E9 Pa; v = 0.38; L = 400mm; B = 300mm; Dia= 2.85mm.

The finite element analysis results for plate of 24mm plate are depicted in Figs. 20 to 24.

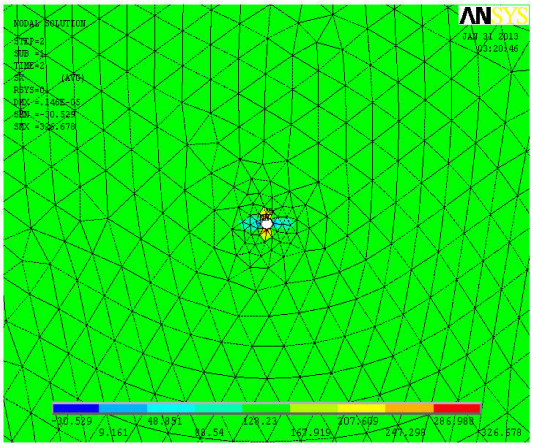

Fig. 20: Finite element model and depiction of X component stresses for 24mm plate

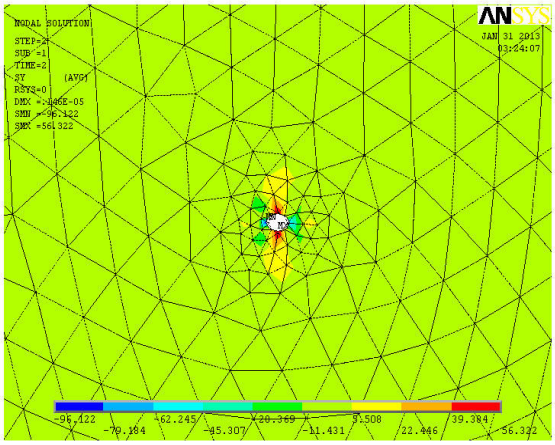

Fig. 21: Finite element model and depiction of Y component stresses for 24mm plate

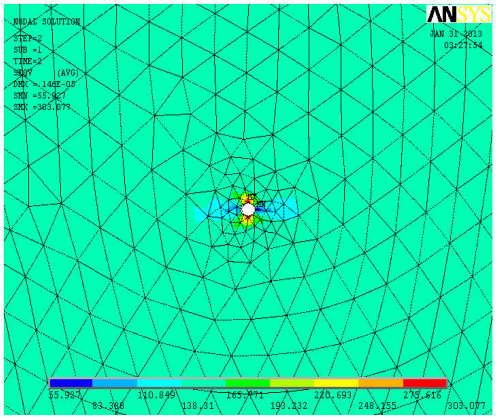

Fig. 22: Finite element model and depiction of von Mises stresses for 24mm plate

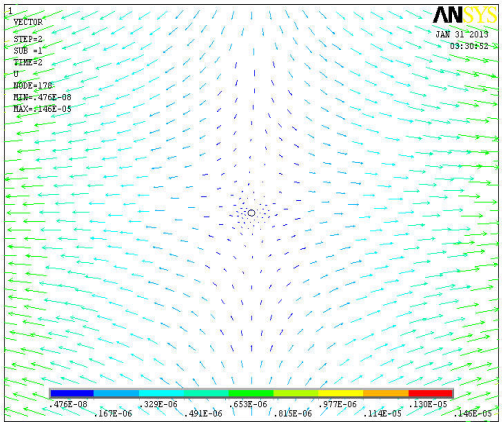

Fig. 23: Finite element model and depiction of vector/displacement plots for 24mm plate

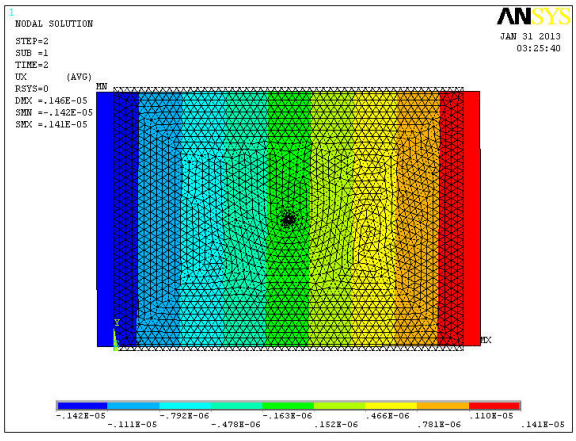

Fig. 24: Finite element model and depiction of Strain for 24mm plate

Fig. 17 giving maximum von Mises of 304.084MPa is a clear indication that as the hole size/thickness increases the strength of materials decreases as shown in Fig. 22 with maximum von Mises stress of 303.077MPa.

Finally the orthogonal stresses of Figs. 15, 16, 20 and 21, show that the composite is stronger in the longitudinal direction. With the results of the orthogonal stresses with the maximum of 304.084MPa, the maximum stress in the material is likely to be greater than 304.084MPa.

5. Conclusion

This work employed a combination of traditional analysis of data and the application of finite element using plane stress analysis to determine the stress distribution of both local and global on the plate subjected to high velocity impact. The major contribution in this work is the consideration of both local and global stress effect.
The stresses, strains and displacements of the discretized nodes were successfully generated and the influence of the parameters mentioned at the periphery of action and boarders of the laminate mesh determined. It is noticed that the maximum influence of the stress was experienced around the incident hole and the minimum at the exterior boarders of the sample. The size of the sample considered was 300mm x 400mm squared. It was observed that; as the diameter of the bullet or hole increases, the values of the stresses, strains and displacements increase.

References

[1]. Cantwell, W.J. & Morton, J. (1989). Comparison of Low Velocity & High Velocity Impact Response of CERP Composites, 20, 545–51.
[2]. Prewo, K.M. (1980). The Importance of Fibres in Achieving Impact Tolerant Composites. Phil. Trans. R. Soc. London, A 294, 551 – 58.
[3]. Gower, H.L., Cronin, D.S., and Plumtree, A. (2008). Ballistic Impact Response of Laminate Conposite Panels. International Journal of Impact Engineering, Vol. 35, pp 1000-1008.
[4]. Sasikumar, M., and Sundareswaran, V. (2013). Ballistic Impact Behavior of Unidirectional Fibre Reinforced Composites. International Journal of Impact Engineering, Vol. 63, pp 164-176.
[5]. Gama, B.A., and Gillespie, J.W. (2011). Finite Element Modeling of Impact, Damage Evolution and Penetration of Thick-Section Composites. International Journal of Impact Engineering, Vol. 38, pp 181-197.
[6]. Wang, J., and Bartholomeusz, R. (2004). Ballistic Damage in Carbon/Epoxy Composite Panels. Journal of Battlefield Technology, Vol. 7, Issue 1, pp 7-13.
[7]. Silva, M.A.G., Cismasiu, C., and Chiorean, C.G. (2005). Numerical Simulation of Ballistic Impact on Composite Laminates. International Journal of Impact Engineering, Vol. 31, pp 289-306.
[8]. Naik, N.K., and Shrirao, P. (2004). Composite Structures under Ballistic Impact. Composite Structures, Vol. 66, pp 579-590.
[9]. Zohdi, T.I., and Powell, D. (2006). Multiscale Construction and Large-Scale Simulation of Structural Fabric Undergoing Ballistic Impact. Composite Methods in Applied Mechanics and Engineering, Vol. 195, pp 94-109.
[10]. Fawaz, Z., Zheng, W., and Bhedinan, K. (2004). Numerical Simulation of Normal and Oblique Ballistic Impact on Ceramic Composite Armour. Composite Structures, Vol. 63, pp 387-395.
[11]. Smith, P.D., and Hetherlington, J.G. (1994). Blast and Ballistic Loading of Structures. Butterworth-Heinemann Ltd, London.
[12]. Abrate, S. (1998). Impact on Laminated Composites: Recent Advances. Applied Mechanical Review, Vol. 4711, pp. 517-544.
[13]. Johnson, G.R. (1976). “Analysis of Elastic-Plastic Impact Involving Severe Distortions”, Journal Of Applied Mechanics, Vol. 43, No. 3, Trans. Asme, Vol. 98, Series E, Sept. pp 439 – 444.
[14]. Zienkiewicz, O.C., (1971) the Finite-Element Method in Engineering Science, McGraw-Hill, New York, N.Y.
[15]. Abrate, S. (2007), Ballistic Impact on Composites. 16th International Conference on Composite materials, Kyoto Japan, pp 1–10.
[16]. Cantwell, W.J. & Morton, J. (1991). The Impact Resistance of Composite Materials: A Review Composites, Vol. 22, pp 347 – 362.
[17]. Lee, S.W.R., and Sun, C.T. (1993) Dynamic Penetration of Graphite Epoxy Laminates Impacted by a Blunt-Ended Projectile. Comp. Sci. Tech., Vol. 49, pp 369-380.

[18]. Ghashghai –Abdi, E., and Moyer E,T. (1984). On the solution of problems involving impact type loading. In Yuceoglu U. & Hessser R., editors, Advances in Aerospace science and engineering, pages 39-48, new York, A.S.M.E Aerospace Division, American Society of Mechanical Engineers.
[19]. Houde, M.J.I. (1990). Impact force model for composite materials. Masters thesis, University of Toronto, Downeview, University of Toronto Institute of Aerospace Studies.
[20]. Bacharach, W.E., and Hansen .R.S. (1998). Mixed Finite-Element Method For Composite Cylinder Subjected To Impact. A.I.A.A. Journal, Vol. 27, Issue 5, pp 632-638.
[21]. Ross, C.A., Malvern, L.E., Sierakowki R.L., and Takeda N. (1985). Finite-element analysis of interlaminar shear stress due to local impact. In recent Advances in composites in the united states and japan, pages 355-367, Philadelpia. American Society for Testing and Materials, ASTM STP 864.
[22]. Chang, F.K., Choi, H.Y., and Wu, H.T. (1991). A New Approach Towards Understanding Damaged Mechanisms and Mechanics Of Laminated Composites Due to Low-Velocity Impact; II- Analysis. Journal Of Composite Materials, Vol. 25, Pp 1012-1038.
[23]. Sun C.T. (1977). An Analytical Method For Evaluation Of Impact Damage Energy Of Laminated Composites. In Composite Materials: Testing and Design. Fourth Conference, Pages 427-440. American Society for Testing And Materials, ASTM STP 617.
[24]. Sun, C.T., and Chen, J.K. (1985). On the impact of initially stressed composite laminates. Journal of composite materials, Vol. 19, pp 490-504.
[25]. Sun, C.T., and Huang, S.N. (1975). Transverse impact problems by higher order beam finite element. Computers and structures, 5: 297-303, 1975.
[26]. Humphreys, E.A. (1981). Development of An Engineering Analysis Of Progressive Damage In Composite During Low Velocity Impact. N.A.S.A., Contract Report N.A.S.A CR-165778, N.A.S.A., Langley Research center, Hampton, Virginia.
[27]. Humphrey, E.A., and Goering, A. (1983). Development Of An Analytic Procedure To Calculate Damage Accumulation In Composites During Low Velocity Impact, NASA Contract Report NASA CR- 166086, N.A.S.A. Langley Research Centre, Hampton, Virginia.
[28]. Donald, F. (2003). Required Engineering in Practice. Proceedings of 11th International IEEE Requirement Engineering Conference. Software Engineering Institute, Carnegie, Melton University.
[29]. Astley, R.J. (1992). Finite Elements of Solids and Structures: An Introduction, 1st edition, Chapman and Hall, London.
[30]. Chandrupatla, T.R. and Belegundu, A.D. (2007) Introduction to Finite Elements in Engineering. 3rd Ed. Prentice-Hall of India (Private Limited), New Delhi-110 001, Pp 1-8.